small methods
www.small-methods.com

Facile Peptide Macrocyclization and Multifunctionalization via Cyclen Installation

Tsz-Lam Cheung, Leo K. B. Tam, Wing-Sze Tam, Leilei Zhang, Hei-Yui Kai, Waygen Thor, Yue Wu, Pak-Lun Lam, Yik-Hoi Yeung, Chen Xie, Ho-Fai Chau, Wai-Sum Lo, Tao Zhang, and Ka-Leung Wong**

Cyclen-peptide bioconjugates are usually prepared in multiple steps that require individual preparation and purification of the cyclic peptide and hydrophilic cyclen derivatives. An efficient strategy is discovered for peptide cyclization and functionalization toward lanthanide probe via three components intermolecular crosslinking on solid-phase peptide synthesis with high conversion yield. Multifunctionality can be conferred by introducing different modular parts or/and metal ions on the cyclen-embedded cyclopeptide. As a proof-of-concept, a luminescent Eu^{3+} complex and a Gd^{3+}-based contrasting agent for in vitro optical imaging and in vivo magnetic resonance imaging, respectively, are demonstrated through utilizing this preparation of cyclen-embedded cyclic arginylglycylaspartic acid (RGD) peptide.

T.-L. Cheung, W.-S. Tam
Department of Chemistry
Hong Kong Baptist University
224 Waterloo Road, Kowloon Tong, Kowloon, Hong Kong China

L. K. B. Tam, H.-Y. Kai, W. Thor, Y. Wu, P.-L. Lam, Y.-H. Yeung, H.-F. Chau, W.-S. Lo, K.-L. Wong
Department of Applied Biology and Chemical Technology
The Hong Kong Polytechnic University
Hung Hom, Kowloon, Hong Kong China
E-mail: klgwong@polyu.edu.hk

L. Zhang, T. Zhang
MOE Key Laboratory of Laser Life Science & Institute of Laser Life Science and College of Biophotonics
South China Normal University
Guangzhou 510631, China
E-mail: zt@scnu.edu.cn

Y. Wu
Department of Surgery
The Chinese University of Hong Kong
Sha Tin, Hong Kong China

C. Xie
Department of Clinical Oncology
University of Hong Kong
Pok Fu Lam, Hong Kong Island, Hong Kong China

The ORCID identification number(s) for the author(s) of this article can be found under https://doi.org/10.1002/smtd.202400006

DOI: 10.1002/smtd.202400006

1. Introduction

Peptide, owing to its excellent biocompatibility, enhanced tissue penetration, ease of modification, and low immunogenicity,[1] has been utilized as therapeutics since the first medical use of insulin in 1922.[2] To date, around 80 FDA-approved peptide-based drugs have entered the global market with more than 150 peptides in clinical development.[3] Apart from being the modulator of intracellular protein–protein interactions (PPI),[4] anticancer and antibacterial agents,[5,6] numerous peptide sequences have been identified with high affinity to specific receptors with the aid of phage display technology.[7,8] Compared to its conformationally flexible linear counterpart, cyclopeptide shows dramatic proteolytic stability conferred by structural rigidity, enhanced bioactivity, better cell permeability, and increased binding affinity.[9–12] Numerous macrocyclization strategies, such as lactamization[13]/lactonization,[14] ring-closing metathesis,[15] Diels-Alder cycloaddition,[16] disulfide bridge formation,[17] click chemistries,[18] and multi-component reactions,[10] have been developed in the past few decades to introduce conformational constraints in short- and medium-size peptides.[19] Meanwhile, peptide functionalization is also crucial for the development of diseased tissue-specific therapeutics,[20] diagnostics,[21] and theranostics,[22] in particular for conjugating targeting peptides to the functional motifs. Therefore, chemists have strived for years to develop simple, efficient, and chemoselective strategies to synthesize functionalized cyclopeptides. Generally, two-component macrocyclization involving a pre-functionalized staple linker[23] or a modifiable staple linker bearing a functional motif for post-cyclization functionalization[24,25] is adopted. For example, Spring and co-workers developed the double-click stapling of diazido peptides using pre-functionalized dialkynyl linkers.[18] However, there are inherent limitations such as the tedious synthetic work of the staple linker with limited functionality and the independent module preparation of stapler, peptide, and functional motif. Another less common practice developed in recent years is to cyclize the peptide with the functional motif and incorporate it in the backbone of the staple linker.[26,27] Perrin and co-workers introduced the crosslinking of *ortho*-phthalaldehyde (OPA) with an amine and thiol to generate a fluorescent isoindole-bridged cyclopeptide.[28]

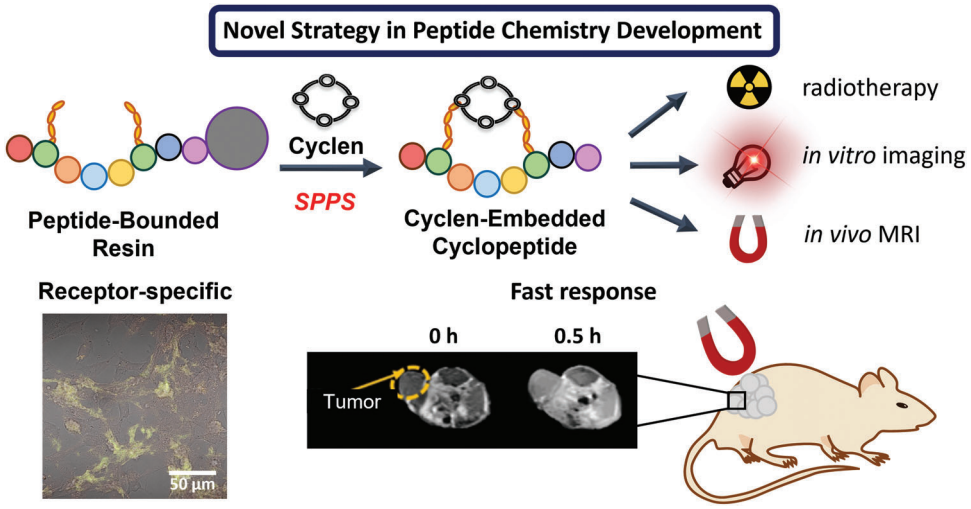

Figure 1. Schematic representation of the diverse biomedical applications for cyclen-embedded peptide macrocyclization strategy in radiotherapy, receptor-specific in vitro luminescence imaging, and fast responding in vivo MRI.

Nonetheless, only single-purpose functionality is achieved upon cyclization with the corresponding motif.

To circumvent this problem, we developed the first versatile multifunctionalized cyclen-embedded peptide stapling strategy (**Figure 1**). Cyclen (1,4,7,10-tetraazacyclododecane) derivatives such as DOTA (1,4,7,10-tetraazacyclododecane-1,4,7,10-tetraacetic acid) exhibit robust kinetic inertness and thermodynamic stability in metal coordination.[29,30] With numerous commercial sources and well-established protocols for modifying cyclen building blocks, these macrocyclic ligands can also be diversely functionalized upon antenna installation and/or lanthanides and transition metals complexation, introducing varieties of potent biomedical applications such as luminescence imaging,[31,32] magnetic resonance imaging (MRI),[29] positron emission tomography (PET), and radiotherapy.[33] The most common practice to prepare cyclen-peptide bioconjugates is that the highly water-soluble lanthanide bioimaging or MRI probe and the linear/cyclic peptide are individually synthesized and purified before their conjugation in aqueous phase through amide bond formation[34–38] or click chemistry.[39,40] Another less common approach is to install the lanthanide probe directly on the linear peptide via solid-phase peptide synthesis.[41–44] Nevertheless, peptide cyclization and probe installation are achieved in multiple steps, rendering its efficiency and cost-effectiveness in green chemistry. Although cyclen-peptide conjugates have been widely reported and well-summarized for improving tumor-specific theranostic outcomes,[45] cyclen derivatives have never been applied to form direct crosslinking on peptides and serve simultaneously as multifunctional ligands.

We report in this work an efficient cyclen-embedded peptide macrocyclization strategy via three components intermolecular crosslinking to prepare cyclopeptide at high conversion yields and with a range of functionalities upon different modular parts or/and metal ion installation. Cyclen is used as the backbone of the stapled linker for peptide macrocyclization on the solid phase and at the same time as a metal chelator. This functionalized cyclopeptide can be further incorporated with an antenna and/or simply coordinated with different lanthanide ions as a probe for biomedical applications. As a proof-of-concept, an arginyl-glycylaspartic acid (RGD) peptide, which binds preferentially to $\alpha_v\beta_3$ integrin that is overexpressed in angiogenesis and tumor metastasis,[46] is cyclized using our cyclen-embedded strategy, followed by lanthanide complexation to give an antenna-equipped Eu^{3+} cancer diagnostic probe and a Gd^{3+}-based contract agent for in vitro luminescent imaging and in vivo MRI, respectively.

2. Results and Discussion

Considering lysine residues (Lys, K) have good nucleophilicity and bear long flexible side chains that favor intermolecular crosslinking, the cyclization method is initially demonstrated on a resin-bound KRGDK peptide **1** with a 4-methoxyphenylacetyl capped N-terminal (**Scheme 1**). The two amine groups on the Lys side chains were then coupled with bromoacetic acid (20 equiv.) in the presence of DIC (20 equiv.) in DMF to give the bromo-functionalized resin-bound peptide **2** as the key intermediate. The optimized cyclization condition of 16 h with 1.5 equiv. of commercially available cyclen building block 1,7-bis(tert-butoxycarbonylmethyl)-1,4,7,10-tetraazacyclododecane **3a** was adopted to obtain the desired cyclen-embedded cyclic KRGDK peptide (**cyc-RGD**) (Table S4, Supporting Information). Alternatively, a modular approach for post-cyclization functionalization can be achieved by incorporating a bis-Alloc protected cyclen building block **3b** with resin-bounded peptide **2**, as this methodology restricted side reactions in each step and gave high conversion yields. Functional modulators can be introduced to the two secondary amines on cyclen after the removal of the Alloc protecting groups with reference to the modified standard protocol.[47] In this case, a well-known carbostyril (cs)-based antenna **5** that sensitizes a series of lanthanide ions[48] was integrated with resin-bounded peptide **4b** to obtain **cyc-RGD-cs** (conv. 68%) after global cleavage as a ligand for luminescent lanthanide probes. The course of the formation was monitored step-by-step by HPLC and ESI-MS to demonstrate the

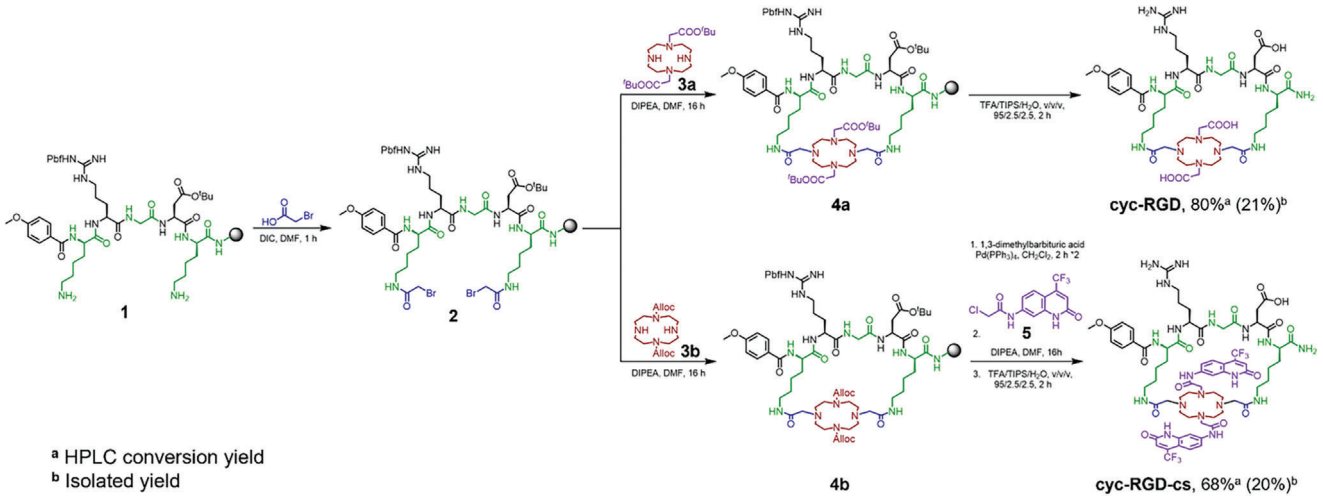

Scheme 1. The synthetic scheme of cyclen-embedded cyclopeptides **cyc-RGD** and **cyc-RGD-cs** constructed on resin-bound RGD peptide.

perfect conversion of **cyc-RGD** and **cyc-RGD-cs** under the optimal condition (Figure S1, Supporting Information).

Luminescent lanthanide imaging offers remarkable advantages over conventional fluorescent imaging for the enhancement of signal-to-noise ratio due to the distinct emission peaks, large ligand-induced Stokes shifts, and long-lived luminescence.[49] The antenna-containing cyclopeptide **cyc-RGD-cs** can coordinate with various trivalent lanthanide ions to yield **Ln-cyc-RGD-cs** which gives luminescence in the visible and/or near-infrared (NIR) range (**Figure 2a**). Our cyclopeptide was found to sensitize the visible luminescence of Eu^{3+}, NIR luminescence of Yb^{3+}, and the dual luminescence of Sm^{3+}. All of them showed characteristic emission profiles in the HEPES buffer at room temperature (Figure 2b-d).[31]The photophysical properties, emission lifetime, q-value,[50] quantum yield,[51,52] and brightness[53] of **Eu-cyc-RGD-cs**, **Sm-cyc-RGD-cs**, and **Yb-cyc-RGD-cs** are summarized in **Table 1**.

It is imperative to assess the cytotoxicity of **Eu-cyc-RGD-cs** before utilizing it as an $\alpha_v\beta_3$-specific imaging probe at the cellular level, and this was investigated by MTT assay in $\alpha_v\beta_3$-overexpressed human bladder carcinoma cell line T24 and human glioblastoma cell line U-87 MG cell lines and the normal human lung fibroblast MRC-5 cell lines. As shown in Figure S5 (Supporting Information), **Eu-cyc-RGD-cs** was non-cytotoxic up to 100 μM in all cell lines, revealing the high biocompatibility of our complex. To examine the $\alpha_v\beta_3$-specific targeting, T24 cells, U-87 MG and MRC-5 cell lines were first incubated with 50 μM of **Eu-cyc-RGD-cs** in either McCoy's 5A (Modified) Medium (for T24 cells) or in Minimum Essential Medium (for U-87 MG and MRC-5), followed by the immunoluminescence imaging of $\alpha_v\beta_3$ in these cell lines after fixation (Figure 2e). It is noteworthy that a comparatively high concentration was used due to the relatively low brightness of our complexes when compared with other lanthanide complexes with the same cs-based antenna.[48] The results indicated the red emission signal of **Eu-cyc-RGD-cs** co-localized well with the green signal from the $\alpha_v\beta_3$ antibody in $\alpha_v\beta_3$-overexpressed T24 (Pearson coefficient: 0.784) and U-87 MG cell lines (Pearson coefficient: 0.470), while negligible signals could only be observed in normal MRC-5 cell line with low $\alpha_v\beta_3$-expression. The overall results demonstrated that **Eu-cyc-RGD-cs** could serve as a safe and $\alpha_v\beta_3$-targeting cancer luminescent imaging probe.

The multifunctionalities of **cyc-RGD** can be achieved simply by coordinating with different metals or their radioisotopes (**M-cyc-RGD**) (**Figure 3a**). DOTA-chelating radionuclides, including ^{68}Ga, ^{64}Cu, ^{90}Y, and ^{177}Lu, are commonly used in PET and radiotherapy.[54] With the cyclen backbone, **cyc-RGD** can strongly chelate to the non-radiative isotopes of Ga^{3+}, Cu^{2+}, Y^{3+}, and Lu^{3+} ions respectively. These isotopes were chelated using the established protocols with the addition of 0.5 equiv. of the corresponding metal ions and ≈50% conversion can be observed (Figure 3b), suggesting **M-cyc-RGD** can be a potential $\alpha_v\beta_3$-targeting radiopharmaceutical upon radiolabelling. Besides, **cyc-RGD** can undergo complexation with Gd^{3+} ions to give **Gd-cyc-RGD** as an MRI contrast agent. As the lanthanidecounterpart showed minimal cytotoxicity in vitro, we further assessed the in vivo capability of **Gd-cyc-RGD** for its potential use as an MRI contrast agent. The proteolytic stability against trypsin at 37 ^{0}C of **Gd-cyc-RGD** and its control, linear KGRDK peptide **1**, (Scheme 1) was first evaluated. While peptide **1** almost completely decomposed within 4 h, 51% of **Gd-cyc-RGD** remained intact (Figure 3c). The enhanced protease resistance of cyclopeptide-based **Gd-cyc-RGD** than the linear peptide 1 due to its constrained structure is expected to improve the body circulation time and tumor targeting.

On the other hand, the kinetic stability which reflects the extent of metal leaching was examined. **Gd-cyc-RGD** and its control, FDA-approved MRI contrast agent Dotarem (**Gd-DOTA**) were incubated in 0.1N HCl (pH = 1) over a period of 24 h and the acid-catalyzed decomplexation process was monitored by HPLC (for **Gd-cyc-RGD**) or LC/MS (for **Gd-DOTA**).[55] As shown in Figure S6 (Supporting Information), **Gd-cyc-RGD** almost remained intact while ca. 10% of **Gd-DOTA** was degraded. To further understand the thermodynamic stability of **Gd-cyc-RGD**, a competition assay was performed with a well-known and strong lanthanide chelator, diethylenetriamine pentaacetate (DTPA).[56] Upon incubation with or without 10, 100, 500, or 1000 equiv. of DTPA for 24 h, negligible decomposition of **Gd-cyc-RGD** was observed (Figure S7, Supporting Information), which was

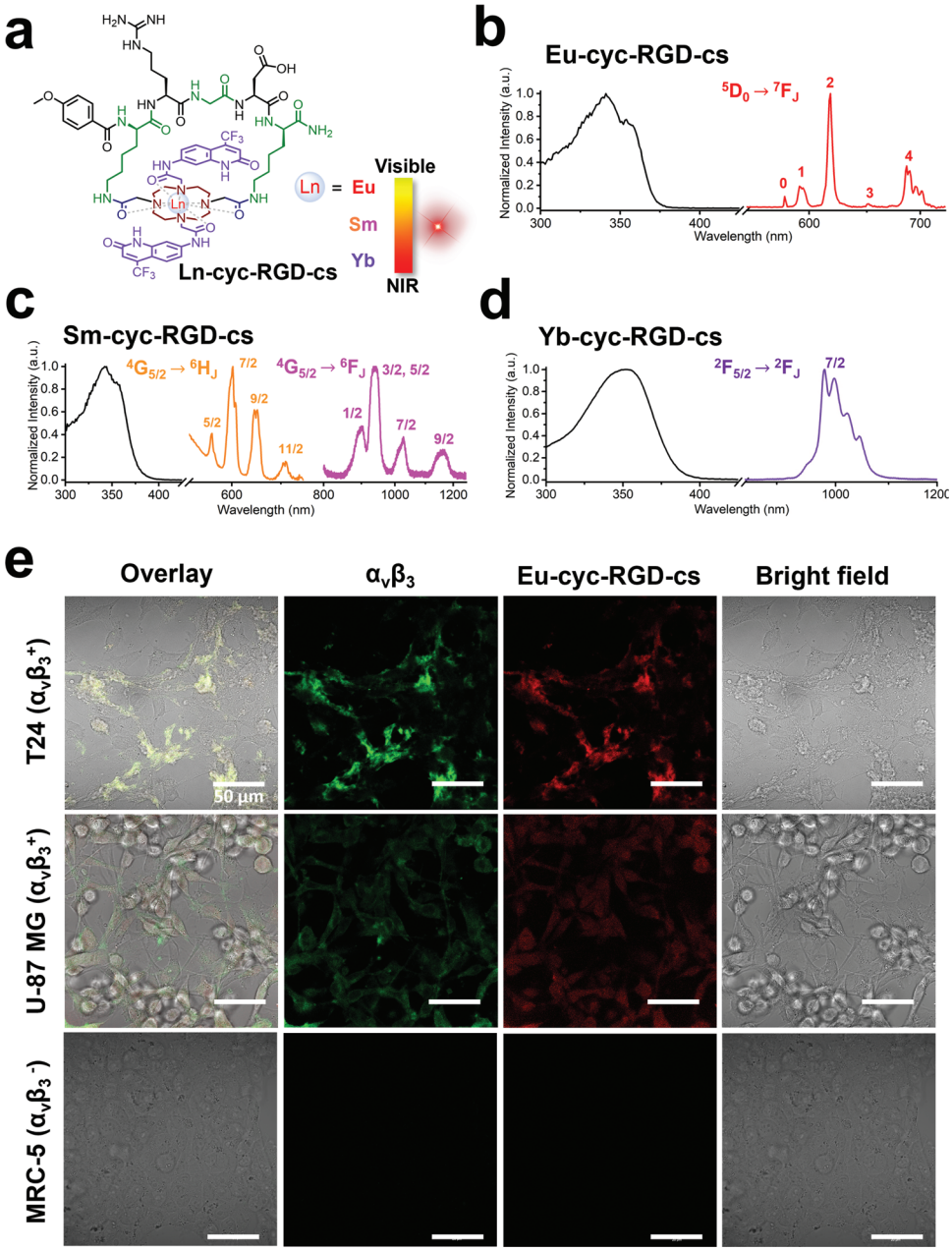

Figure 2. a) General structure of **Ln-cyc-RGD-cs** for visible to NIR luminescent imaging upon different metals coordination. The normalized excitation (in black) and emission spectra (in color) of b) **Eu-cyc-RGD-cs** (20 μM), c) **Sm-cyc-RGD-cs** (30 μM), and d) **Yb-cyc-RGD-cs** (84 μM) in 10 mM HEPES buffer measured at room temperature. e) Immunoluminescence imaging of $\alpha_v\beta_3$ in T24 ($\alpha_v\beta_3^+$), U-87 MG ($\alpha_v\beta_3^+$) and MRC-5 ($\alpha_v\beta_3^-$) cells after incubation of 50 μM **Eu-cyc-RGD-cs** in medium for 24 h (scale bar: 50 μm).

Table 1. The photophysical properties, luminescence lifetime (τ), q-value, quantum yield (Φ), and brightness (BR) of **Ln-cyc-GRD-cs**.

Complex	λ_{ex} [nm]	ϵ [$\times 10^3$ M^{-1} cm^{-1}]	λ_{em} [nm]	τ (H_2O)[b] [ms]	τ (D_2O)[b] [ms]	ϕ_{Ln}[c] [%]	BR[d] [M^{-1} cm^{-1}]
Eu-cyc-RGD-cs[a]	340	8.01	580, 592, 618, 651, 687	0.640	1.409	1.67	134
Sm-cyc-RGD-cs	342	9.60	564, 602, 644, 710, 901, 938, 1027, 1161	0.018	0.032	0.04	3.84
Yb-cyc-RGD-cs	351	2.41	981, 998, 1021, 1043	0.013	0.069	0.07	1.69

[a] The q-value is determined as 0.91, which is calculated by $3.02 \times [\tau\ (H_2O)^{-1} - \tau\ (D_2O)^{-1} - 0.25 - 0.075x]$ (x = number of amide N–H oscillators);[50] [b] Determined from the corresponding emission decay curve; [c] Relative to the corresponding standard $Ln(TTA)_3$ complexes;[51,52] [d] Calculated from BR = attenuation coefficient × quantum yield.[53]

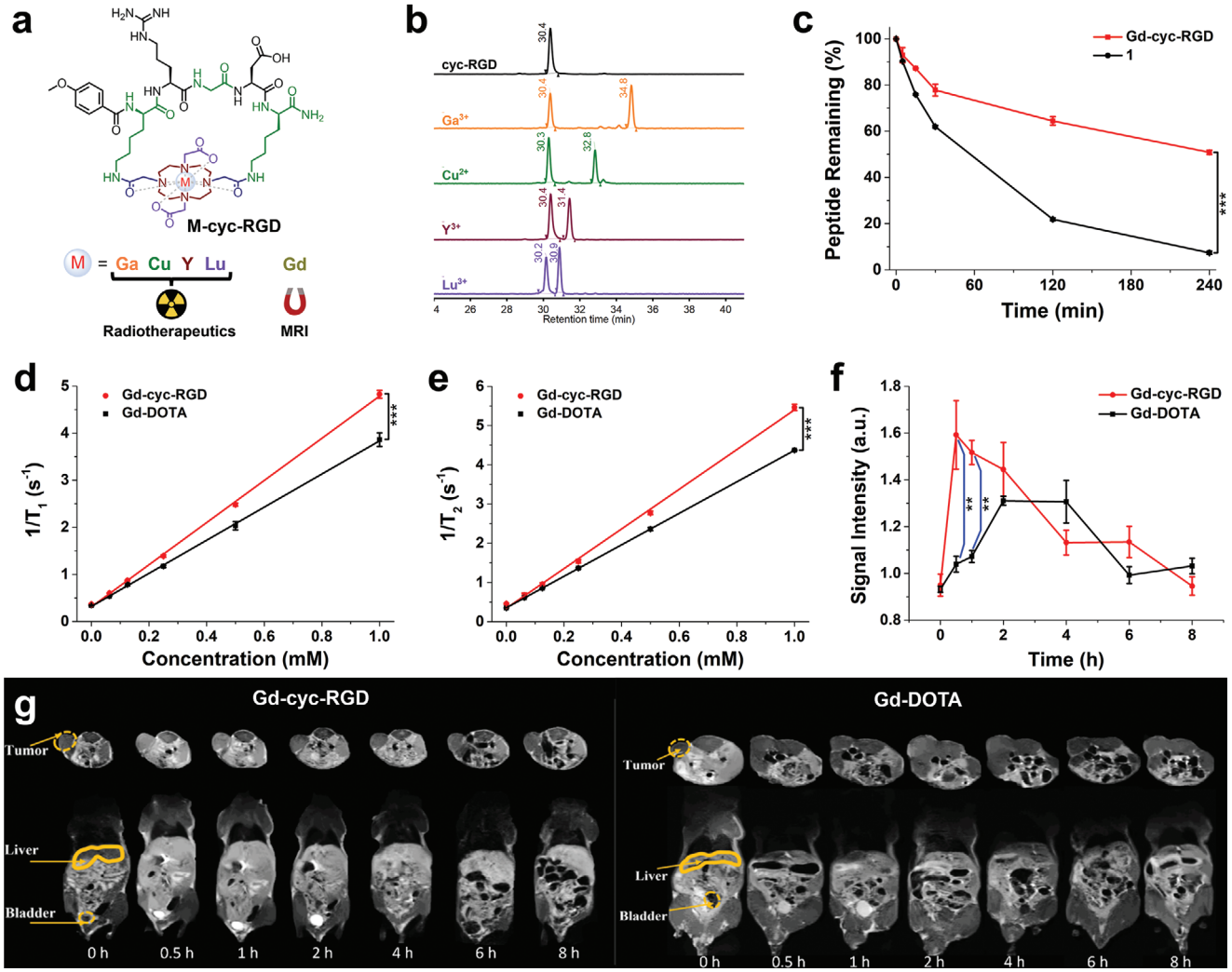

Figure 3. a) General structure of **M-cyc-RGD** and its potential biomedical applications upon different metal coordination. b) HPLC chromatograms of non-radioactive isotope labeling of **M-cyc-RGD**. c) Stability tests of **Gd-cyc-RGD** and peptide **1** against enzymatic peptide degradation as monitored by HPLC. Peptide remaining (%) was calculated by Δcomplex/ΣΔmixture. d) Relaxation rates $1/T_1$ and e) $1/T_2$ versus **Gd-cyc-RGD** and **Gd-DOTA** concentrations. f) Quantification of T_1 contrast enhancement of **Gd-cyc-RGD** and **Gd-DOTA** in tumor over 8 h. g) T_1-weighted MRI scans of $\alpha_v\beta_3$-positive U-87 MG cell tumor xenografts in nude mice treated with 0.1 mmol kg^{-1} of **Gd-cyc-RGD** or **Gd-DOTA** over a period of 8 h. Data are expressed as the mean ± standard deviation (SD) of three independent experiments. $^{**}p < 0.01$ and $^{***}p < 0.001$ as calculated by the Student's *t*-test.

comparable to **Gd-DOTA** under the same conditions, suggesting no ligand displacement occurred even at a high concentration of competitors. It is worth mentioning that these stability-related assays were also performed with **Eu-cyc-RGD-cs** and the results showed it was highly stable in both acidic environments and high concentrations of DTPA (Figures S6 and S7, Supporting Information). In our metal complexes, two or four carboxylate sidechains were replaced by amides when compared with the typical DOTA chelator. It is believed that the locked amide sidechains of the cyclen for peptide cyclization reduce the chance for the outer species to interact with the coordinated metal ion which minimizes the metal leaching upon acid digestion or ligand displacement. All these results suggested our metal complexes provided high and comparable kinetic inertness and thermodynamic stability with lanthanide-DOTA complex for safe biological applications.

To evaluate the effectiveness of **Gd-cyc-RGD** for MRI, the longitudinal relaxivities (r_1) and transverse relaxivities (r_2) were measured at 20 ^{0}C and 1.4 T using **Gd-DOTA** as control. As shown in Figure 3d,e, **Gd-cyc-RGD** (r_1 = 4.47 and r_2 = 5.06 mM^{-1} s^{-1}) showed better MRI-contrasting ability compared to **Gd-DOTA** (r_1 = 3.52 and r_2 = 4.07 mM^{-1} s^{-1}). Lastly, the in vivo MRI contrasting ability of the **Gd-cyc-RGD** and **Gd-DOTA** was studied and compared in $\alpha_v\beta_3$-positive U-87 MG cell tumor-cell xenograft mouse models. As shown in Figure 3g, T_1-weighted MR images of the tumor-bearing mice were captured at various time points within 8 h upon intravenous injection (both at 0.1 mmol kg^{-1}). For **Gd-cyc-RGD**, a fast response was observed with the signal intensity on the tumor site reaching its maximum after 0.5 h post-injection and remaining high until 1 h post-injection. Instead, **Gd-DOTA** required a longer response time for 2 h post-injection, which is four times slower than **Gd-cyc-RGD** (Figure 3f). The

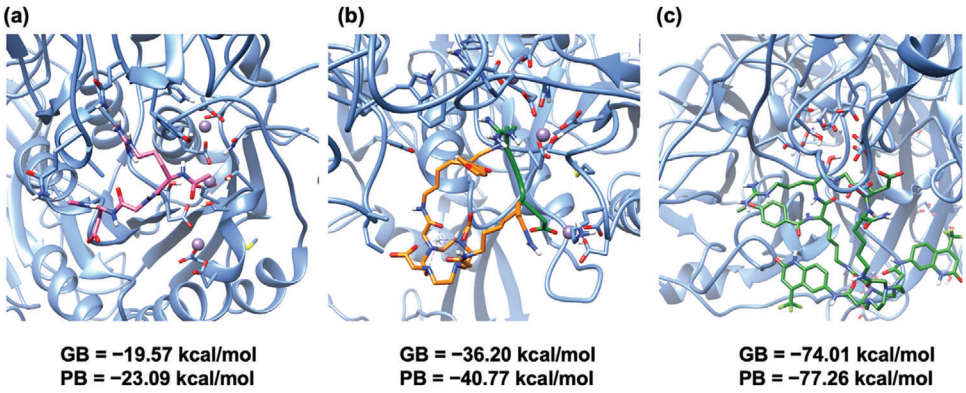

Figure 4. The representative conformations of a) linear RGD peptide, b) **Y-cyc-RGD**, and c) **Y-cyc-RGD-cs** (using Y^{3+} as an analog for Gd^{3+} and Eu^{3+} to avoid spin contamination) with $\alpha_v\beta_3$ protein (blue) over 100 ns of molecular dynamics simulation. The calculated generalized Born (GB) and Poisson-Boltzmann (PB) values represent the binding free energy.

half-an-hour effective period and higher maximum signal intensity of **Gd-cyc-RGD** over **Gd-DOTA** on the tumor site were contributed by its higher relaxivity and preference to be retained in $\alpha_v\beta_3$-overexpressed tumors owing to the presence of the cyclic KRGDK peptide. All these features concluded that **cyc-RGD** can be functionalized as a promising MRI contrast agent.

Computational modeling and simulations were conducted to study the binding between **Gd-cyc-RGD** or **Eu-cyc-RGD-cs** (using Y^{3+} as an analog for Gd^{3+} and Eu^{3+} to avoid spin contamination) and $\alpha_v\beta_3$ integrin using Molecular Mechanics Poisson-Boltzmann/Generalized Born Surface Area (MMPBSA/MMGBSA) calculation.[57] The binding free energies in terms of Generalized Born (GB) and Poisson-Boltzmann (PB) values, were found to be −36.20 and −40.77 kcal mol^{-1} respectively for the optimized structure of **Y-cyc-RGD** (**Figure 4**), which were remarkably lower than that of the linear RGD peptide (GB = −19.57 kcal mol^{-1}; PB = −23.09 kcal mol^{-1}). A much stronger binding energy between **Y-cyc-RGD-cs** and $\alpha_v\beta_3$ integrin (GB = −74.01 kcal mol^{-1}; PB = −77.26 kcal mol^{-1}) was also calculated to support the high specificity of this probe toward $\alpha_v\beta_3$-overexpressed cancer cells. In addition, **Y-cyc-RGD** was calculated to have a similar binding pocket to the linear RGD peptide[58] with $\alpha_v\beta_3$ integrin (Figure S12, Supporting Information), revealing a strong binding between **Y-cyc-RGD** and $\alpha_v\beta_3$ integrin which is consistent with our results above.

3. Conclusion

In summary, we have developed a novel and highly efficient solid-phase synthetic strategy for preparing multifunctional cyclen-embedded cyclopeptides. The cyclopeptides can be transformed into different theranostic agents through coordination with different metal ions. As a concept-proofing model, a cyclic KRGDK peptide can be either transformed into an in vivo MRI contrast agent (**Gd-cyc-RGD**) or a luminescent bioimaging tool (**Eu-cyc-RGD-cs**) that can be utilized as an in vitro probe which specifically binds to $\alpha_v\beta_3$ integrin in cancer cells. This work not only suggests the great potential of cyclen as a staple linker but also provides an invaluable addition to the peptide macrocyclization and multifunctionalization toolbox.

Supporting Information

Supporting Information is available from the Wiley Online Library or from the author.

Acknowledgements

All animal experiments were carried out in accordance with the National Institutes of Health (NIH) Guidelines for the Care and Use of Laboratory Animals of South China Normal University (Reference no. SCNU-BIP-2024-027). Financial assistances from the Hong Kong Research Grants Council No. 12300021, NSFC/RGC Joint Research Scheme (N_PolyU209/21), and the Centre for Medical Engineering of Molecular and Biological Probes (AoE/M-401/20) are gratefully acknowledged (K.-L. W). We also appreciate the service of high-resolution mass spectrometry (HRMS) provided by The University Research Facility in Life Sciences (ULS) and Ho-Nam Mak from the Department of Applied Biology and Chemical Technology of The Hong Kong Polytechnic University for the HRMS analysis.

Conflict of Interest

The authors declare no conflict of interest.

Data Availability Statement

The data that support the findings of this study are available in the supplementary material of this article.

Keywords

$\alpha_v\beta_3$ integrin, cyclen-peptide conjugates, lanthanides, luminescence, solid phase peptide synthesis

Received: January 2, 2024
Revised: March 28, 2024
Published online: April 9, 2024

[1] F. Araste, K. Abnous, M. Hashemi, S. M. Taghdisi, M. Ramezani, M. Alibolandi, *J. Control. Release* **2018**, *292*, 141.

[2] I. Vecchio, C. Tornali, N. L. Bragazzi, M. Martini, *Front. Endocrinol.* **2018**, *9*, 613.
[3] M. Muttenthaler, G. F. King, D. J. Adams, P. F. Alewood, *Nat. Rev. Drug Discov.* **2021**, *20*, 309.
[4] L.-G. Milroy, T. N. Grossmann, S. Hennig, L. Brunsveld, C. Ottmann, *Chem. Rev.* **2014**, *114*, 4695.
[5] W. Chiangjong, S. Chutipongtanate, S. Hongeng, *Int. J. Oncol.* **2020**, *57*, 678.
[6] Y. Huan, Q. Kong, H. Mou, H. Yi, *Front. Microbiol.* **2020**, *11*, 582779.
[7] B. P. Gray, K. C. Brown, *Chem. Rev.* **2014**, *114*, 1020.
[8] R. Liu, X. Li, W. Xiao, K. S. Lam, *Adv. Drug Deliv. Rev.* **2017**, *110*, 13.
[9] J. A. Schneider, T. W. Craven, A. C. Kasper, C. Yun, M. Haugbro, E. M. Briggs, V. Svetlov, E. Nudler, H. Knaut, R. Bonneau, M. J. Garabedian, K. Kirshenbaum, S. K. Logan, *Nat. Commun.* **2018**, *9*, 5114.
[10] L. Reguera, D. G. Rivera, *Chem. Rev.* **2019**, *119*, 9836.
[11] X. Li, S. Chen, W. D. Zhang, H. G. Hu, *Chem. Rev.* **2020**, *120*, 10079.
[12] Y. H. Lau, P. DeAndrade, Y. Wu, D. R. Spring, *Chem. Soc. Rev.* **2015**, *44*, 91.
[13] A. D. DeAraujo, H. N. Hoang, W. M. Kok, F. Diness, P. Gupta, T. A. Hill, R. W. Driver, D. A. Price, S. Liras, D. P. Fairlie, *Angew. Chem. Int. Ed.* **2014**, *53*, 6965.
[14] A. Parenty, J.-M. Campagne, X. Moreau, *Chem. Rev.* **2006**, *106*, 911.
[15] P. M. Cromm, J. Spiegel, T. N. Grossmann, *ACS Chem. Biol.* **2015**, *10*, 1362.
[16] J. E. Montgomery, J. A. Donnelly, S. W. Fanning, T. E. Speltz, X. Shangguan, J. S. Coukos, G. L. Greene, R. E. Moellering, *J. Am. Chem. Soc.* **2019**, *141*, 16374.
[17] H. Y. Chow, Y. Zhang, E. Matheson, X. Li, *Chem. Rev.* **2019**, *119*, 9971.
[18] Y. H. Lau, Y. Wu, P. DeAndrade, W. R. J. D. Galloway, D. R. Spring, *Nat. Protoc.* **2015**, *10*, 585.
[19] E. A. Villar, D. Beglov, S. Chennamadhavuni, J. A. Porco, D. Kozakov, S. Vajda, A. Whitty, *Nat. Chem. Biol.* **2014**, *10*, 723.
[20] B. M. Cooper, J. Legre, D. H. O' Donovan, M. Ö. Halvarsson, D. R. Spring, *Chem. Soc. Rev.* **2021**, *50*, 1480.
[21] X. Sun, Y. Li, T. Liu, Z. Li, X. Zhang, X. Chen, *Adv. Drug Deliv. Rev.* **2017**, *110*, 38.
[22] X.-L. Hu, N. Kwon, K.-C. Yan, A. C. Sedgwick, G.-R. Chen, X.-P. He, T. D. James, J. Yoon, *Adv. Funct. Mater.* **2020**, *30*, 1907906.
[23] G. K. Dewkar, P. B. Carneiro, M. C. T. Hartman, *Org. Lett.* **2009**, *11*, 4708.
[24] N. Assem, D. J. Ferreira, D. W. Wolan, P. E. Dawson, *Angew. Chem. Int. Ed.* **2015**, *54*, 8665.
[25] J. Ceballos, E. Grinhagena, G. Sangouard, C. Heinis, J. Waser, *Angew. Chem. Int. Ed.* **2021**, *60*, 9022.
[26] Y. Wu, H.-F. Chau, W. Thor, K. H. Y. Chan, X. Ma, W.-L. Chan, N. J. Long, K.-L. Wong, *Angew. Chem. Int. Ed.* **2021**, *60*, 20301.
[27] Y. Wu, H.-F. Chau, Y.-H. Yeung, W. Thor, H.-Y. Kai, W.-L. Chan, K.-L. Wong, *Angew. Chem. Int. Ed.* **2022**, *61*, e202207532.
[28] M. Todorovic, K. D. Schwab, J. Zeisler, C. Zhang, F. Bénard, D. M. Perrin, *Angew. Chem. Int. Ed.* **2019**, *58*, 14120.
[29] J. Wahsner, E. M. Gale, A. Rodríguez-Rodríguez, P. Caravan, *Chem. Rev.* **2019**, *119*, 957.
[30] S. Wang, T.-Z. Wu, H.-J. Park, T. Peng, L.-X. Cao, S. K. Mellerup, G.-Q. Yang, N. Wang, J.-B. Peng, *Adv. Opt. Mater.* **2016**, *4*, 1882.
[31] J. C. G. Bünzli, *Chem. Rev.* **2010**, *110*, 2729.
[32] S. Shinoda, *Chem. Soc. Rev.* **2013**, *42*, 1825.
[33] T. J. Wadas, E. H. Wong, G. R. Weisman, C. J. Anderson, *Chem. Rev.* **2010**, *110*, 2858.
[34] S. Lacerda, É. Toth, *ChemMedChem* **2017**, *12*, 883.
[35] J. A. González-Vera, D. Bouzada, C. Bouclier, M. E. Vázquez, M. C. Morris, *Chem. Commun.* **2017**, *53*, 6109.
[36] H. F. Schmitthenner, T. M. Barrett, S. A. Beach, L. E. Heese, C. Weidman, D. E. Dobson, E. R. Mahoney, N. C. Schug, K. G. Jones, C. Durmaz, O. Otasowie, S. Aronow, Y. P. Lee, H. D. Ophardt, A. E. Becker, J. P. Hornak, I. M. Evans, M. C. Ferran, *ACS Appl. Bio Mater.* **2021**, *4*, 5435.
[37] M. Isaac, A. Pallier, F. Szeremeta, P.-A. Bayle, L. Barantin, C. S. Bonnet, O. Sénèque, *Chem. Commun.* **2018**, *54*, 7350.
[38] D. Parker, J. D. Fradgley, K.-L. Wong, *Chem. Soc. Rev.* **2021**, *50*, 8193.
[39] L. M. De León-Rodríguez, Z. Kovacs, *Bioconjugate Chem.* **2008**, *19*, 391.
[40] M. Cieslikiewicz-Bouet, S. V. Eliseeva, V. Aucagne, A. F. Delmas, I. Gillaizeau, S. Petoud, *RSC Adv.* **2019**, *9*, 1747.
[41] L. Connaha, G. Angelovski, *Org. Chem. Front.* **2020**, *7*, 4121.
[42] G. Fremy, L. Raibaut, C. Cepeda, M. Sanson, M. Boujut, O. Sénèque, *J. Inorg. Biochem.* **2020**, *213*, 111257.
[43] S. Laine, J.-F. Morfin, M. Galibert, V. Aucagne, C. S. Bonnet, É. Tóth, *Molecules* **2021**, *26*, 2176.
[44] J.-H. Choi, G. Fremy, T. Charnay, N. Fayad, J. Pécaut, S. Erbek, N. Hildebrandt, V. Martel-Frachet, A. Grichine, O. Sénèque, *Inorg. Chem.* **2022**, *61*, 20674.
[45] L. M. DeLeón-Rodríguez, Z. Kovacs, *Bioconjugate Chem.* **2008**, *19*, 391.
[46] F. Danhier, A. Le Breton, V. Préat, *Mol. Pharmaceutics* **2012**, *9*, 2961.
[47] F. Wojcik, S. Mosca, L. Hartmann, *J. Org. Chem.* **2012**, *77*, 4226.
[48] D. Kovacs, X. Lu, L. S. Mészáros, M. Ott, J. Andres, K. E. Borbas, *J. Am. Chem. Soc.* **2017**, *139*, 5756.
[49] H.-F. Chau, Y. Wu, W.-Y. Fok, W. Thor, W. C.-S. Cho, P. Ma, J. Lin, N.-K. Mak, J.-C. G. Bünzli, L. Jiang, N. J. Long, H. L. Lung, K.-L. Wong, *JACS Au* **2021**, *1*, 1034.
[50] L. Dai, W.-S. Lo, Y. Gu, Q. Xiong, K.-L. Wong, W.-M. Kwok, W.-T. Wong, G.-L. Law, *Chem. Sci.* **2020**, *10*, 4550.
[51] A. I. Voloshin, N. M. Shavaleev, V. P. Kazakov, *J. Photochem. Photobiol., A* **2000**, *136*, 203.
[52] M. P. Tsvirko, S. B. Meshkova, V. Y. Venchikov, Z. M. Topilova, D. V. Bol'shoi, *Opt. Spectrosc.* **2001**, *90*, 669.
[53] K.-L. Wong, J. C. G. Bünzli, P. A. Tanner, *J. Lumin.* **2020**, *224*, 117256.
[54] Z. Baranyai, G. Tircsó, F. Rösch, *Eur. J. Inorg. Chem.* **2020**, *1*, 35.
[55] T. J. Clough, L. Jiang, K.-L. Wong, N. J. Long, *Nat. Commun.* **2019**, *10*, 1420.
[56] E. Debroye, T. N. Parac-Vogt, *Chem. Soc. Rev.* **2014**, *43*, 8178.
[57] T. Hou, J. Wang, Y. Li, W. Wang, *J. Chem. Inf. Model.* **2011**, *51*, 69.
[58] J. F. van Agthoven, J.-P. Xiong, J. L. Alonso, X. Rui, B. D. Adair, S. L. Goodman, M. A. Arnaout, *Nat. Struct. Mol. Biol.* **2014**, *21*, 383.

